Res Chem Intermed (2016) 42:5653–5664
DOI 10.1007/s11164-015-2393-7

Dye-sensitized solar cells based on two-dimensional TiO_2 nanosheets as the scattering layers

Caiyun Wu[1] · Lihong Qi[1] · Yujin Chen[1] · Qiuyun Ouyang[1] · Chunyan Li[1]

Received: 28 November 2015 / Accepted: 11 December 2015 / Published online: 2 January 2016

Abstract Two-dimensional (2D) TiO_2 nanosheets with high crystallinity and good light scattering properties were synthesized via a simple solvothermal process using reduced graphite oxide as a sacrificing template. X-ray diffraction patterns and electron microscopy images indicated that the prepared 2D TiO_2 nanosheets were composed of high-crystalline anatase TiO_2 nanoparticles. Then, the 2D anatase TiO_2 nanosheets were used as a scattering layer of the photoelectrode, which is expected to produce high-efficiency dye-sensitized solar cells (DSSCs). Compared with ones with pure TiO_2 nanoparticle photoelectrodes, DSSCs based on 2D TiO_2 nanosheets as middle scattering layer yield the highest photoelectrical conversion efficiency of 7.54 %. This is because the obtained 2D TiO_2 nanosheets have excellent light scattering, allowing for fast interfacial charge transfer, the least series resistance, and the best charge collection efficiency. These have been systematically evidenced by the electrochemical impedance spectra, intensity-modulated photocurrent spectroscopy and intensity-modulated photovoltage spectroscopy.

Keywords TiO_2 nanosheets · Template · Scattering layer · Interfacial charge transfer · Charge collection efficiency

Introduction

Since the pioneering work by Grätzel in 1991, dye-sensitized solar cells (DSSCs) have attracted much attention for their low cost, easy fabrication, and high power-conversion efficiency (η) [1–4]. Generally, a standard photoelectrode is one of the most important prerequisites for highly efficient DSSCs because photoelectrodes not

✉ Lihong Qi
qilihong@126.com

[1] College of Science, Harbin Engineering University, Harbin 150001, People's Republic of China

only function for dye sensitizer load and photoelectron transport but also allow the electrolytes to diffuse into the anchored dyes [5, 6]. Therefore, extensive efforts have been made to design and prepare excellent photoelectrode materials, possessing a packed property of faster electron transfer and more lighting scattering [7–9]. However, it is still difficult to simultaneously meet these two criteria within one photoelectrode [10].

Generally, films based on nanocrystalline TiO_2 particles have been used as a photoelectrode owing to their high surface area for enough dye molecule loading [11, 12]. However, the small particle size ($\sim$20 nm) results in negligible light scattering, which led to the low photon absorption [13, 14]. Recently, much scattering layer research has been done to improve the light harvesting of dye sensitizers via lengthening the photon transport pathway. One is to choose nanowire, nanorod, nanobelt, or large particles, which are added into the nanocrystalline TiO_2 particle matrix, or on the top of nanoparticluate TiO_2 film as a scattering layer [15–18]. The other one is to use hierarchical TiO_2 nanostructures as a light scattering layer, such as mesoporous TiO_2 beads, nanoporous TiO_2 spheres or aggregates and hollow microspheres [19–23]. However, the low surface area as well as the manufactured complexity of these scattering materials greatly limits their applications in DSSCs. Therefore, it is greatly eager if one could to introduce unique TiO_2 nanostructures with a simple method, as an efficient light scattering layer.

Recently, two-dimensional (2D) TiO_2 nanomaterials have attracted much attention because of their unique electrical and optical properties [24–26]. Due to its efficient stacking from zero-dimensional nanoparticles, 2D TiO_2 nanomaterials would be good at dye adsorption and light scattering. The conventional 2D TiO_2 nanostructures are prepared using hydrofluoric (HF) acid as a capping and shape-controlling agent [27, 28]. However, HF is a kind of unfriendly and corrosive chemical agent; it is urgent to synthesize 2D TiO_2 nanostructures without fluorine. Sacrificing template may be a good method to obtain 2D nanostructure. For example, Kim et al. synthesized 2D disk-shaped TiO_2 using ethyl cellulose as a sacrificing template, and DSSCs based on it as a scattering layer obtained higher power conversion efficiency [29]. However, the size of disk-shaped TiO_2 is relatively small, which makes the light scattering less efficient. Preparation of 2D TiO_2 nanomaterials with large size could further improve the properties of light scattering.

In this work, anatase TiO_2 nanosheets with high crystallinity and good light scattering property have been prepared via a simple solvothermal method. The reduced graphite oxide (rGO) has been in situ prepared as a sacrificing template for the synthesis of 2D TiO_2 nanosheets. Then, anatase TiO_2 nanosheets were applied as an efficient scattering layer incorporated in DSSCs. Consequently, the DSSCs based on the 2D anatase TiO_2 nanosheet scattering layer photoelectrode exhibit high photoelectrical conversion efficiency (7.54 %). This is much higher than those of DSSCs based on traditional pure small TiO_2 nanoparticles (7.22 %). Characterizations such as electrochemical impedance spectra (EIS), intensity-modulated photocurrent spectroscopy (IMPS), and intensity-modulated photovoltage spectroscopy (IMVS) have been carried out to explore the intrinsic electron transfer and light harvesting mechanism.

Experimental section

Synthesis of TiO_2 nanosheets with rGO as a sacrificing template

The typical 2D anatase TiO_2 nanosheets with high crystallinity were obtained via a simple solvothermal process using rGO as sacrificing template. Firstly, graphite oxide (GO) was synthesized via the Hummers method [30]. Then, certain mass ratios of HNO_3, tetrabutyl titanate (TBT), and GO (0.5 wt %) were dissolved and dispersed in ethanol with some amount of hexadecyl trimethyl ammonium bromide (CTAB) as a surfactant. Thirdly, the solution was transferred into a Teflon-lined autoclave at 180 °C for 12 h. Finally, the TiO_2-rGO composite was obtained after the products were collected by centrifugation and washed with ethanol. At last, the samples were sintered at 360 °C (ramp of 1 °C min^{-1}) in H_2 atmosphere for 6 h to get highly crystalline TiO_2-rGO composite [31], and 500 °C (ramp of 1 °C min^{-1}) in air for 6 h in turn to remove rGO template and get 2D anatase TiO_2 nanosheets. After the sample is sintered in the H_2 atmosphere, TiO_2 nanocrystals could be better dispersed in the surface of rGO, which resulted in the formation of TiO_2 nanosheets.

Fabrication of photoelectrodes and DSSCs assembly

Two kinds of TiO_2 pastes were obtained by mixing 3 ml of TiO_2 colloid with 680 mg of TiO_2 nanoparticles (P25, Degussa) or anatase TiO_2 nanosheets, respectively. The TiO_2 colloid was prepared according to previously published work [32]. Two kinds of photoelectrodes were fabricated: electrodes with a two-layer TiO_2 nanoparticle (labeled as C1), and electrodes with TiO_2 nanoparticle as underlayer and outlayer, and one-layer TiO_2 nanosheet middle layer as scattering layer (labeled as C2). The 2D TiO_2 nanosheets were designed as the middle layer of the photoelectrode for further usage of the light. There also have some reports about this structure [33]. Both electrodes were sintered at 450 °C for 30 min. The dye sensitization of photoelectrode and the DSSC fabrication are according to the literature [5]. The structure characterization and photoelectrical measurement details followed the standard route.

Results and discussion

Structural characterization of TiO_2 nanosheet

The XRD pattern of the as-prepared anatase TiO_2 nanosheet is shown in Fig. 1. Nine Bragg diffraction peaks ($2\theta = 25.2°$, 37.7°, 48.0°, 53.8°, 55.0°, 62.7°, 68.9°, 70.2°, and 75.1°) of a typical pattern of anatase phase could be clearly observed (JCPDS No. 21-1272), which are indexed as (101), (004), (200), (105), (211), (204), (116), (220), and (215), respectively. No other diffraction peaks are observed, which indicates that the TiO_2 nanosheets are pure anatase phase. Also, the Raman spectrum is also carried out to characterize the composition of TiO_2. The Raman

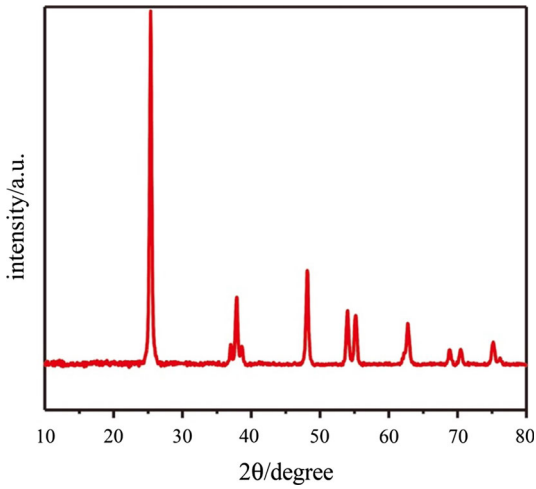

Fig. 1 Wide-angle XRD patterns of anatase TiO_2 nanosheets

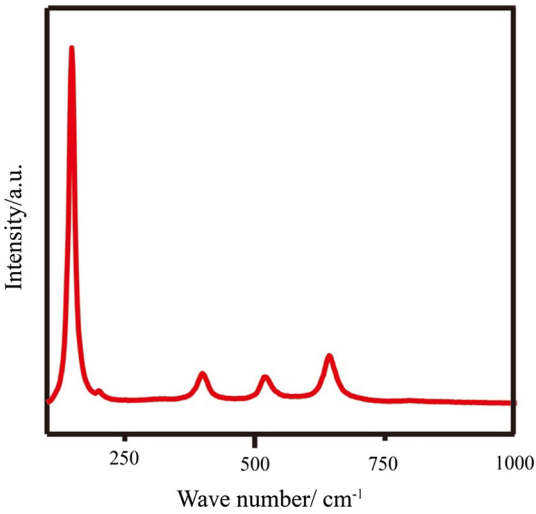

Fig. 2 Raman spectrum of anatase TiO_2 nanosheets

technique is considered to be a helpful tool to distinguish the different phases of TiO_2 [34]. Figure 2 shows the Raman spectrum of the obtained sample. We can clearly see four high-intensity Raman responding peaks at 148, 395, 512, and 641 cm^{-1}, which could be ascribed to E_g, B_{1g}, $A_{1g}(B_{1g})$, and E_g modes of anatase TiO_2 nanomaterials, respectively. Furthermore, the TG curve of TiO_2 nanosheets is also shown in Fig. 3. It could be clearly seen that the sample has no weight loss above 100 °C, which proved that rGO has been completely removed from the sample.

With rGO as a sacrificing agent, the TiO_2 nanosheet with a big size has been obtained. It was made up of small-size TiO_2 nanoparticles with high crystallinity and compact connection among them. The average size of the nanoparticles is 8 nm.

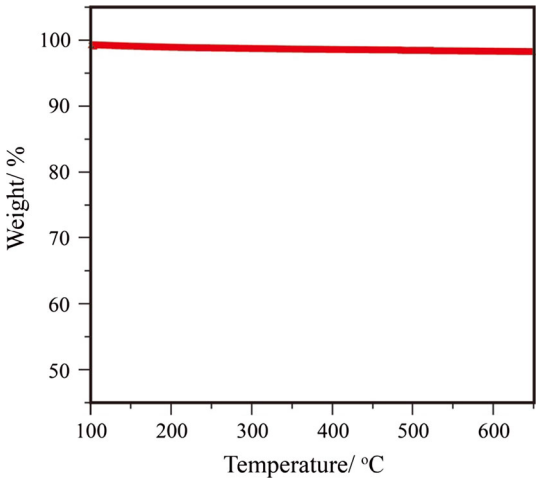

Fig. 3 TG curve of the as-prepared anatase TiO_2 nanosheets

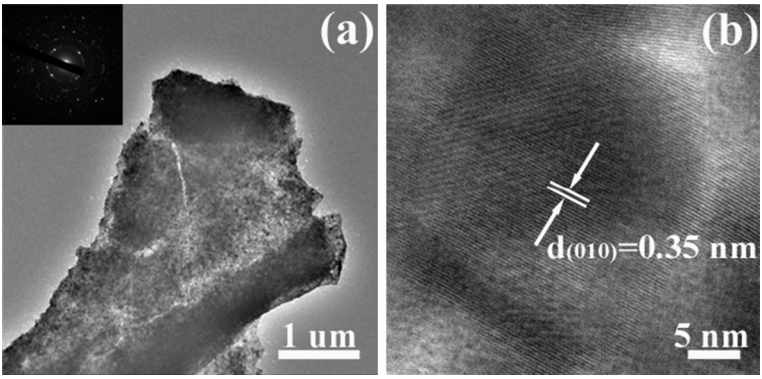

Fig. 4 TEM and HRTEM image of TiO_2 nanosheets

Measurement of the lattice fringes also gives a d spacing of 0.35 nm, which is indexed to the (101) planes of anatase TiO_2 (Fig. 4).

X-ray photoelectron spectroscopy (XPS) was then used to further analyze the chemical valence of the as-prepared samples. The XPS peaks at 460.5 and 529.1 eV (Fig. 5a) can be assigned to the binding energies of Ti 2p, and O 1s, respectively [35]. It indicates that there actually exist Ti and O elements in the compound. No C element exists in the compound. For high-resolution XPS of Ti 2p, there appear two binding energy peaks at ca. 458.2 and 463.6 eV, which could be assigned to the Ti $2p_{3/2}$ and Ti $2p_{1/2}$ (Fig. 5b).

The light scattering property of photoelectrode plays an important role in determining the η of DSSCs, which is evaluated by the DRS. Figure 6 presents the DRS of the naked TiO_2 nanoparticle film, and TiO_2 nanoparticle underlayer and outlayer with the obtained anatase TiO_2 nanosheets as scattering layer film, respectively. Compared with the naked TiO_2 nanoparticle film, film with 2D

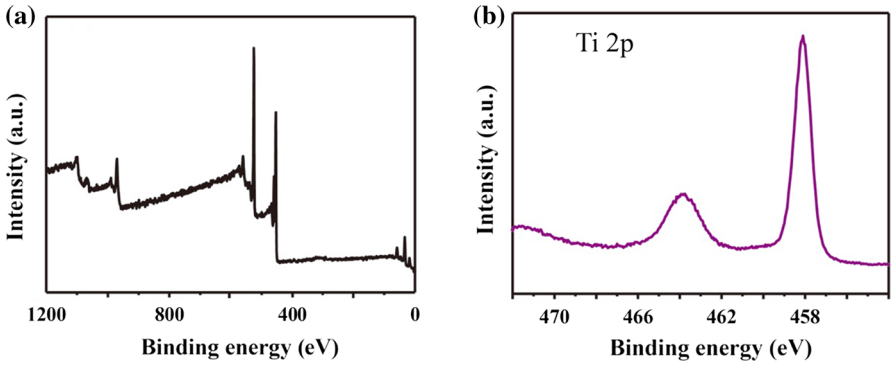

Fig. 5 XPS survey spectra of TiO_2 nanosheets (**a**), high-resolution XPS spectra for TiO_2 nanosheets relative to Ti 2p (**b**)

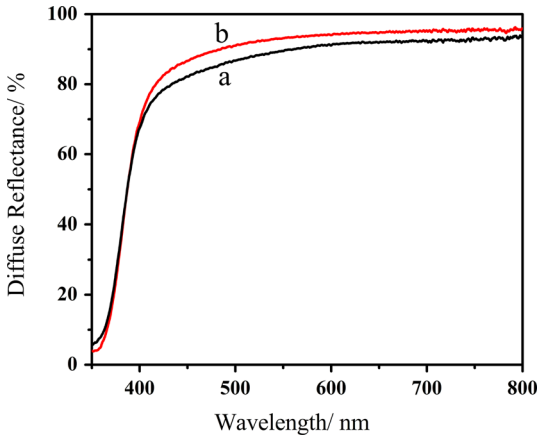

Fig. 6 UV–Vis diffused reflectance spectra (DRS) of TiO_2 nanoparticle film (*a*) and the films based on the TiO_2 nanoparticle underlayer and anatase TiO_2 nanosheets as scattering layer (*b*)

nanosheet shows higher light scattering capability in the visible region from 400 to 800 nm, revealing that the 2D anatase TiO_2 nanosheets have a higher light-scattering effect than the naked TiO_2 nanoparticles. The improved light scattering effect can thus increase the light traveling pathway, which could result in higher light-harvesting efficiency and a corresponding higher photocurrent.

From the above data, it could be concluded that the 2D anatase TiO_2 nanosheets with high crystallinity and good light-scattering properties have been prepared via a facile solvothermal method using rGO as a sacrificing template.

Photoelectrical character of DSSCs with TiO_2 nanosheets as scattering layer

Because 2D TiO_2 nanosheets possess not only good light scattering property but also fast charge transfer, they are a good candidate for the scattering layer of DSSCs. The cross-section SEM images of photoelectrode-based on TiO_2 nanoparticles and TiO_2 nanosheet as scattering layer are shown in Fig. 7. The film thickness

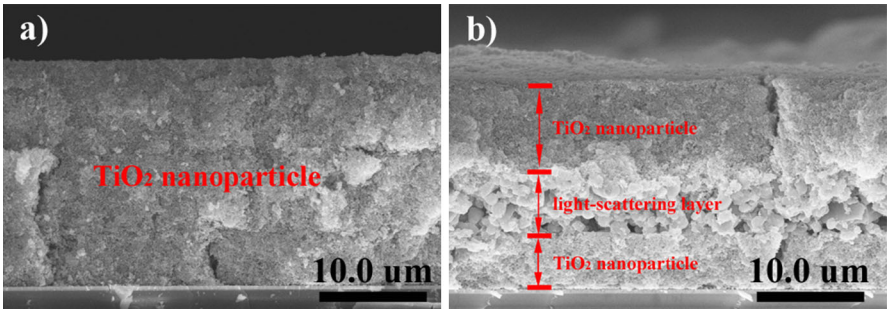

Fig. 7 Cross-sectional SEM images of the photoelectrodes based on TiO_2 nanoparticle film (**a**) and film based on the TiO_2 nanoparticle underlayer and outlayer, and anatase TiO_2 nanosheet as scattering layer (**b**)

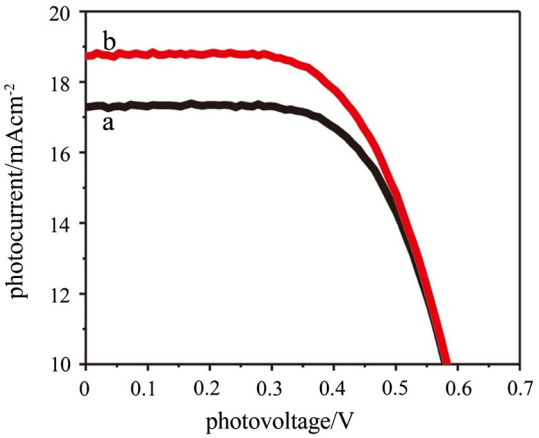

Fig. 8 Photocurrent–photovoltage curves of conventional TiO_2 nanoparticle-based C1 (*a*) and TiO_2 nanosheet-based C2 (*b*) DSSCs, respectively

is ca. 20 μm. The typical photocurrent–photovoltage curves of C1 and C2 are shown in Fig. 8. The values of open circuit voltage (V_{oc}), short-circuit current (J_{sc}), fill factor (FF), and power conversion efficiency (η), obtained from the measured curves, are summarized in Table 1. The J_{sc} and η of C2, which is with TiO_2 nanosheet as scattering layer, are 18.8 mA cm^{-2} and 7.54 %, respectively. Both are all improved compared with these of C1 based on TiO_2 nanoparticles. The increment in J_{sc} may be due to the excellent photoelectron transfer capability of the anatase TiO_2 nanosheet with high crystallinity and better light scattering capability.

The key factors determining the photoelectrical properties

Overall, the photoelectrochemical properties of DSSCs are determined by many factors, such as the dye adsorption amount, photoelectron transport, charge collection efficiency, and so on. The dye unloading measurement was carried out to determine the dye adsorption amount. According to Lambert–Beer law, the molar concentrations of dye in C1 and C2 is calculated as 1.08, and 1.09×10^{-7} mol cm^{-2},

Table 1 Summarized cell performance results of the fabricated DSSCs

Cells	V_{oc} (V)	J_{sc} (mA cm^{-2})	FF	η (%)
C1	0.58	17.3	0.72	7.22
C2	0.58	18.8	0.69	7.54

respectively. So, C2 can realize comparable dye adsorption amount to C1. The adsorbed amount of dye molecules is not the main factor to determine the power conversion efficiency of DSSCs. So, the anatase TiO_2 nanosheet as a light scattering layer plays a significant role in determining the η of DSSCs. To elucidate this, the photoelectron transport rate, series resistance, and charge collection efficiency have been studied by EIS and IMVS/IMPS, respectively.

The electron recombination time (τ_n), the electron transport time (τ_d), and the charge collection efficiency (η_{cc}) are important factors to estimate the overall performance of DSSCs. τ_n and τ_d could be obtained via Eq. (1) and Eq. (2), respectively [9]:

$$\tau_n = \frac{1}{2\pi f_n} \tag{1}$$

$$\tau_d = \frac{1}{2\pi f_d} \tag{2}$$

where f_n and f_d are the characteristic frequency minimum of the IMVS and IMPS imaginary component, respectively. Based on τ_n and τ_d, η_{cc} is also calculated according to the Eq. (3):

$$\eta_{cc} = 1 - \frac{\tau_d}{\tau_n} \tag{3}$$

τ_n, τ_d, and η_{cc} of C1 and C2 are shown in Fig. 9a–c, respectively. Generally, the high η_{cc} will result in high η. C2, which is based on TiO_2 nanosheets as a scattering layer, has shorter τ_d and τ_n. So, it possesses a better charge collection efficiency (η_{cc}) at a different light intensity irradiance than C1. This is because the anatase TiO_2 nanosheets possess comparable dye adsorption and better light scattering capability. Thus, it has the highest η. All of these results match very well with the data of photocurrent–photovoltage curves.

The EIS is a powerful method to research internal resistances for the photoelectron transfer of DSSCs. The wide frequency range of the EIS could measure wide-scale internal resistances simultaneously [36]. EIS can study photoelectron transfer and recombination across the photoelectrode, charge transfer at counter electrode, and the diffusion constant of redox shuttle. Generally, the impedance at low frequency (0.01–1 Hz) reflects the Nernst diffusion of redox shuttle in the electrolyte. The impedance at high frequency (1 k–100 kHz) reflects the charge-transfer resistance at the Pt–redox shuttle interface. The medium-frequency (1–1 kHz) responds to the interface of photoelectrode-dye–redox shuttle electrolyte [37]. The Nyquist plots of the EIS for DSSCs based on different photoelectrodes are shown in Fig. 9d. Also, the equivalent circuit model is shown in Fig. 10. R_s is a series resistance, reflecting the sheet resistance of the TCO, contact

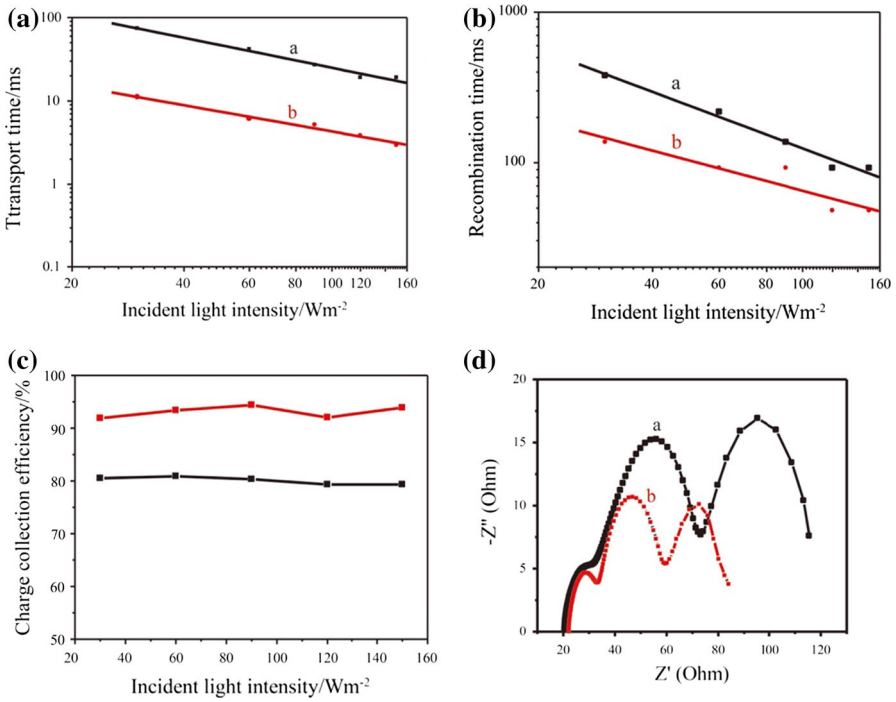

Fig. 9 The IMPS response (**a**), IMVS response (**b**), charge collection efficiency (**c**), and Nyquist diagrams of the impedance spectra (**d**) of conventional TiO_2 nanoparticle-based C1 (*a*) and TiO_2 nanosheet-based C2 (*b*) DSSCs, respectively

resistance, and wire resistance [38]. R_2 represents the charge transfer resistance of interface between the photoelectrode-dye–redox shuttle. C_2 is the capacitance of the same interface. Z_{Dif} represents the Warburg impedance corresponding to the Nernst diffusion of redox shuttle.

According to the equivalent circuit model of Fig. 10, the EIS data are obtained and listed in Table 2. It could be found that R_2, responding to the interfacial resistance of the TiO_2-dye–redox shuttle, is 34.68 Ω for C1 and 18.82 Ω for C2. The lower interface resistance will result in faster interfacial photoelectron transport rate, which favors the higher η. So, C2 has higher η than C1. These results are in accordance with photocurrent–photovoltage and IMVS/IMPS data discussed above.

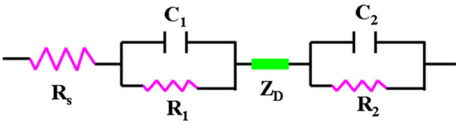

Fig. 10 Equivalent circuit used to represent interfaces in composite solar cells composed of TCO–TiO_2-dye–I_3^-/I^-–Pt–TCO. R and C represent resistance and capacitance, respectively. Z_D represents the Warburg impedance relative to the Nernst diffusion of I_3^- in the electrolyte

Table 2 Detailed EIS parameters for DSSCs made from various photoelectrodes

Cells	R_s (Ω)	R_1 (Ω)	R_2 (Ω)
C1	20.1	0.62	34.68
C2	22.3	0.51	18.82

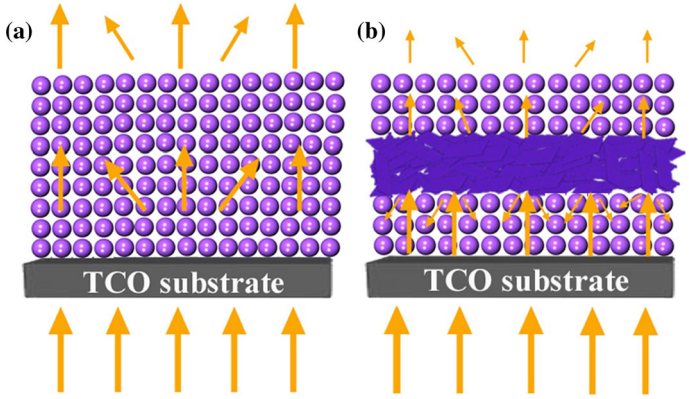

Fig. 11 Light traveling path in the photoelectrode based on the TiO_2 nanoparticle (**a**) and the photoelectrode with anatase TiO_2 nanosheet middle layer as light scattering layer (**b**)

All the results strongly indicate that the prepared anatase TiO_2 nanosheets are good candidates for light scattering layer for DSSCs.

According to the above results, a simple light traveling path model has been proposed to explain the difference of the photoelectrode based on TiO_2 nanoparticles and the photoelectrode with anatase TiO_2 nanosheets as light scattering layer. When light travels through the photoelectrode based on TiO_2 nanoparticles, light is only partially absorbed by the TiO_2 nanoparticles, while a major light directly passes through and is not useful for the generation of photoelectrons (Fig. 11a). For the sake of contrast, when light goes through the photoelectrode based with anatase TiO_2 nanosheets as scattering layer, much light could be reflected into the nanocrystalline TiO_2 underlayer directly by the anatase TiO_2 nanosheets, besides the intrinsic TiO_2 nanoparticle absorption and transmission (Fig. 11b). This could effectively increase the light passing path inside the photoelectrode, resulting in a higher light-harvesting efficiency and a corresponding higher photocurrent density.

Conclusions

In summary, anatase TiO_2 nanosheets with high crystallinity and good light-scattering properties have been synthesized via a simple solvothermal process using reduced graphite oxide as a template. Because of comparable dye adsorption amount and excellent light-scattering capability, the DSSCs based on a photoelectrode with TiO_2 nanoparticle as underlayer and outlayer, and anatase TiO_2

nanosheet as scattering layer got a higher photoelectrical conversion efficiency of 7.54 %, higher than ones based on the naked TiO_2 nanoparticles. The improved η is also ascribed to the fast photoelectron interfacial transport rate and the best charge collection efficiency. These are proved by the EIS and IMVS/IMPS measurements. We believe that our synthetic approach and systematic work pave a new route to prepare the 2D TiO_2 nanosheet structures, where advantages of both comparable dye absorption amount and excellent light scattering property could be integrated into a single material as an efficient scattering layer for further improving the η of DSSCs.

Acknowledgments We gratefully acknowledge the support of this research by the National Natural Science Foundation of China (51302047).

References

1. B. O'Regan, M. Gratzel, Nature **353**, 737 (1991)
2. M. Gratzel, Nature **414**, 338 (2001)
3. U. Bach, D. Lupo, P. Comte, J.E. Moser, F. Weissörtel, J. Salbeck, H. Spreitzer, M. Gratzel, Nature **395**, 583 (1998)
4. M. Grätzel, C. R. Chim. **9**, 578 (2006)
5. M.K. Nazeeruddin, A. Kay, I. Rodicicio, R. Humphry-Baker, E. Müller, P. Liska, N. Vlachopoulos, M. Gratzel, J. Am. Chem. Soc. **115**, 6382 (1993)
6. M. Gratzel, Acc. Chem. Res. **42**, 1788 (2009)
7. Z. Dong, H. Ren, C.M. Hessel, J. Wang, R. Yu, Q. Jin, M. Yang, Z. Hu, Y. Chen, Z. Tang, H. Zhao, D. Wang, Adv. Mater. **26**, 905 (2013)
8. S. Yang, Y. Hou, J. Xing, B. Zhang, F. Tian, X.H. Yang, H.G. Yang, Chem. Eur. J. **19**, 9366 (2013)
9. X. Miao, K. Pan, Y. Liao, W. Zhou, Q. Pan, G. Tian, G. Wang, J. Mater. Chem. A **1**, 9853 (2013)
10. Y. Rui, Y. Li, Q. Zhang, H. Wang, Nanoscale **5**, 12574 (2013)
11. A. Yella, H.W. Lee, H.N. Tsao, C. Yi, A.K. Chandiran, M.K. Nazeeruddin, E.W.G. Diau, C.Y. Yeh, Science **334**, 629 (2011)
12. J. Shen, R. Cheng, Y. Chen, X. Chen, Z. Sun, S. Huang, A.C.S. Appl, Mater. Interfaces **5**, 13000 (2013)
13. D. Kuang, J. Brillet, P. Chen, M. Takata, S. Uchida, H. Miura, K. Sumioka, S.M. Zakeeruddin, M. Grätzel, ACS Nano **2**, 1113 (2008)
14. W. Peng, L. Han, Z. Wang, Chem. Eur. J. **20**, 8483 (2014)
15. Y.Y.W.B. Tan, J. Phys. Chem. B **110**, 15932 (2006)
16. K. Pan, Y. Dong, C. Tian, W. Zhou, G. Tian, B. Zhao, H. Fu, Electrochim. Acta **54**, 7350 (2009)
17. L. Liang, Y. Liu, X.-Z. Zhao, Chem. Commun. **49**, 3958 (2013)
18. S.H. Hwang, J. Roh, J. Jang, Chem. Eur. J. **19**, 13120 (2013)
19. F.Z. Huang, D.H. Chen, X.L. Zhang, R.A. Caruso, Y.B. Cheng, Adv. Funct. Mater. **20**, 1301 (2010)
20. K.Y. Yuan, Y.C. Qiu, W. Chen, M. Zhang, S.H. Yang, Energy Environ. Sci. **4**, 2168 (2011)
21. A. Latini, C. Cavallo, F.K. Aldibaja, D. Gozzi, D. Carta, A. Corrias, L. Lazzarini, G. Salviati, J. Phys. Chem. C **117**, 25276 (2013)
22. F. Huang, D. Chen, Y. Chen, R.A. Caruso, Y.-B. Cheng, J. Mater. Chem. C **2**, 1284 (2014)
23. L.-P. Heiniger, F. Giordano, T. Moehl, and M. Grätzel, Adv. Energy Mater. **4**, 3412 (2014)
24. T. Tachikawa, S. Yamashita, T. Majima, J. Am. Chem. Soc. **133**, 7197 (2011)
25. L. Pan, J.-J. Zou, S. Wang, Z.-F. Huang, A. Yu, L. Wang, X. Zhang, Chem. Commun. **49**, 6593 (2013)
26. N. Roy, Y. Sohn, D. Pradhan, ACS Nano **7**, 2532 (2013)
27. H.G. Yang, G. Liu, S.Z. Qiao, C.H. Sun, Y.G. Jin, S.C. Smith, J. Zou, H.M. Cheng, G.Q. Lu, J. Am. Chem. Soc. **131**, 4078 (2009)
28. J. Pan, G. Liu, G.Q. Lu, H.M. Cheng, Angew. Chem. Int. Ed. **50**, 2133 (2011)
29. C. S. Lee, J. K. Kim, J. Y. Lim, and J. H. Kim, ACS Appl. Mater. Interfaces **1**, 20842 (2014)
30. S. Hummers, R. Offeman, J. Am. Chem. Soc. **80**, 1339 (1958)

31. L. Qi, Y. Ma, Q. Ouyang, Y. Zhang, L. Li, Y. Chen, J. Nanopart. Res. **14**, 907 (2012)
32. K. Pan, Q. Zhang, Q. Wang, Z. Liu, D. Wang, J. Li, Y. Bai, Thin Solid Films **515**, 4085 (2007)
33. Y. Dong, K. Pan, G. Tian, W. Zhou, Q. Pan, T. Xie, D. Wang, H. Fu, Dalton Trans. **40**, 3808 (2011)
34. K. Pan, Y. Dong, W. Zhou, Q. Pan, Y. Xie, T. Xie, G. Tian, G. Wang, A.C.S. Appl, Mater. Interfaces **5**, 8314 (2013)
35. Z. Mou, Y. Wu, J. Sun, P. Yang, Y. Du, C. Lu, A.C.S. Appl, Mater. Interfaces **6**, 13798 (2014)
36. C. Longo, A.F. Nogueira, M.A. De Paoli, H. Cachet, J. Phys. Chem. B **106**, 5925 (2002)
37. J.Y. Zhang, Y.H. Deng, D. Gu, S.T. Wang, L. She, R.C. Che, Z.S. Wang, B. Tu, S.H. Xie, D.Y. Zhao, Adv. Energy Mater. **1**, 241 (2011)
38. J.L. Lan, T.C. Wei, S.P. Feng, C.C. Wan, G.Z. Cao, J. Phys. Chem. C **116**, 25727 (2012)